DSPACE

https://dspace.org/

Comparison of air pollution hotspots in the Highveld using airborne data

Ncipha, Xolile Gerald

2011-06-22
http://hdl.handle.net/10539/10166

Downloaded from a DSpace repository. https://dspace.org/

Chapter 2

Data and Methodology

A brief background of this study is given in this chapter, together with a detailed description of the research aircraft and instruments onboard. Seasonal flight campaigns over the Highveld air pollution hotspots will be summerised. The data collection and analysis of air quality data will be discussed. Meteorological data will also be used to assist in the interpretation of the analysed air quality data.

Project Background

This study was borne out of a project named 'Airborne Monitoring of Greenhouse Gases and other Air Pollutants over South Africa'. The project was conducted by the South African Weather Service (SAWS) and the Climatology Research Group (CRG) from the University of Witwatersrand for the Department of Environmental Affairs and Tourism (DEAT). The project was conducted from April 2004 to March 2006. The main aim of this project was to establish baseline ambient conditions for greenhouse gases as well as criteria and hazardous air pollutants over air pollution hotspots in South Africa.

The air pollution hotspots that were monitored over South Africa were the Highveld, Durban, Richards Bay, Cape Town and the Eastern Cape region. Only data from the Highveld air pollution hotspots monitoring has been used for this study. The Highveld air pollution hotspots monitored were Secunda, Witbank, Rustenburg and the Vaal Triangle, including their surrounding towns. They were monitored in autumn, winter and spring.

Characteristics of the Highveld air pollution hotspots

Air quality over the Highveld air pollution hotspots is affected by emissions from different local sources including industry, agriculture, transport, households, vegetation fires and wind-blown dust (NWDACE, 2002; MDACE, 2003; GDACE, 2004). It is also influenced by air transport into and out of these air pollution hotspots as well as mixing in the atmosphere (Garstang *et al*., 1996; Freiman and Piketh, 2003; Piketh *et al*., 2004). Atmospheric loading of air pollutants over these air pollution hotspots varies at diurnal and seasonal temporal scales. Primary pollutant's diurnal variation is caused by the evolution of the mixing layer (Annegarn *et al*., 1996a). For photochemically produced air pollutants, the diurnal variation is caused by the evolution of the mixing layer and the diurnal variation in solar radiation intensity reaching the earth surface, which is the driving force of photochemical processes (Trainer *et al*., 1987; Poulida *et al*., 1994; Annegarn *et al*., 1996a; Betts *et al*., 2002; Taubman *et al*., 2004). Seasonally the loading is generally higher in winter than in summer. This is due to the stronger emissions from biomass, fossil fuel burning and the slower removal by less efficient photochemical processes in winter (Parish *et al*., 1990; Doddridge *et al*., 1992). The frequent occurrence of high pressure systems in winter worsens the air quality situation in winter (Scheifinger, 1992; Tyson *et al*., 1996; GDACE, 2004). The lower air pollution levels in summer are the results of moist unstable conditions, which are conducive for rapid air pollution dispersion, air mixing, wet deposition by rainfall (Tyson *et al*., 1996; GDACE, 2004), and faster removal by efficient photochemical processes (Parish *et al*., 1990; Doddridge *et al*., 1992).

Location of the major air pollution sources over the Highveld air pollution hotspots

Figures 2.1 to 2.4 identify the major air pollution sources over the Highveld air pollution hotspots using SO_2 an indicator pollutant. SO_2, because of its short atmospheric lifetime (one week or less) its concentration has a large spatial variation, and it is high at or near the source (Seinfeld and Pandis, 2006; WMO, 2006c). This characteristic of SO_2 makes it easy to distinguish or identify point sources from area sources from SO_2 spatial

distribution maps. The data presented in Figures 2.1 to 2.4 is all the data below 1500 m above median topography of the sites. The maximum and median statistical values are calculated for each 0.05 by 0.05 degree grid box. A detailed procedure in developing these spatial maps is given by Piketh *et al*., (2006).

Witbank and its surrounding towns

From the maximum SO_2 values spatial distribution map over Witbank and the surrounding towns (Figure 2.1), three SO_2 hotspots are discernable. They are caused by emissions from four industrial complexes, i.e. Middelburg industries, Witbank and Duvha industries, Lynnville and Clewer industries and Ogies and Kendal industries. The positions of these SO_2 hotspots coincide with the positions of industrial complexes identified in the land use map of Witbank and the surrounding towns (Figure 1.1). Around these industrial complexes there are residential places that emit SO_2 from fossil fuel burning for cooking and space heating (Piketh *et al*., 2006).

Secunda and its surrounding towns

From the Secunda and surrounding towns SO_2 spatial distribution map (Figure 2.2), in the maximum SO_2 values map, industrial sources are easily distinguishable. They are positioned at Matla, Kriel, Tutuka and Secunda. All four of these sites house coal-fired power stations (MDALA, 2005). SO_2 concentrations above 250 ppb were detected over these industrialised sites. From the median SO_2 values spatial distribution map (Figure 2.2) over Secunda and surrounding sites, an area source signature can be seen starting at Leandra stretching southwards to southwest of Charl Cilliers. This SO_2 area source may be attributed to domestic fossil fuel burning emissions from townships over that area.

Rustenburg and its surrounding towns

From the Rustenburg and surrounding towns SO_2 spatial distribution map (Figure 2.3), in the maximum SO_2 values spatial distribution map, two industrial point sources are discernible, one east of the Rustenburg city and one over Ga-Luka area. SO_2 concentrations in excess of 120 ppb were detected over these two industrial sites. The

two SO_2 hotspots positions coincide with the positions of industrial and mining sites identified in the land use map of Rustenburg and the surrounding towns (Figure 1.3). From the median SO_2 values spatial distribution map (Figure 2.3) over Rustenburg and surrounding sites, two area sources are discernible. In Figure 1.3 the area sources correspond with the combination of industrial, urban and township sites, which are Photsaneng, Kanana, Rustenburg city and Phokeng. The wide SO_2 spatial distribution over these areas are due to the combination of industrial, city and domestic fossil fuel burning emissions from townships. SO_2 concentration in the median values over these area sources is in excess of 10 ppb.

The Vaal Triangle area and its surrounding towns

From the Vaal Triangle area and surrounding towns SO_2 spatial distribution map (Figure 2.4), in the maximum SO_2 values map, SO_2 concentration values in excess of 300 ppb were detected just south of Vereeniging from industrial emissions. The industrial complex south of Vereeniging showed SO_2 spatial distribution that was greater than 200 ppb. The other two industrial sites at Sasolburg and Vanderbijlpark showed SO_2 values exceeding 150 ppb. There is another source east of Meyerton which showed values about 150 ppb. From the median SO_2 values spatial distribution map (Figure 3.4), three unkown sources with point source shape are easily discernable. One over Deneysville and two at the locations (-26.6'S, 28.2E) and (-26.7'S, 28.2E). From the median SO_2 values spatial distribution map (Figure 2.4), there is a signature of area sources starting north of Evaton extending to the south of Vereeniging. These area sources positions coincide with the positions of townships around Evaton, Vereeniging, and industries around them (Figure 1.4). These area sources are due to a combination of emissions from industries, the city and domestic fossil fuel burning from townships.

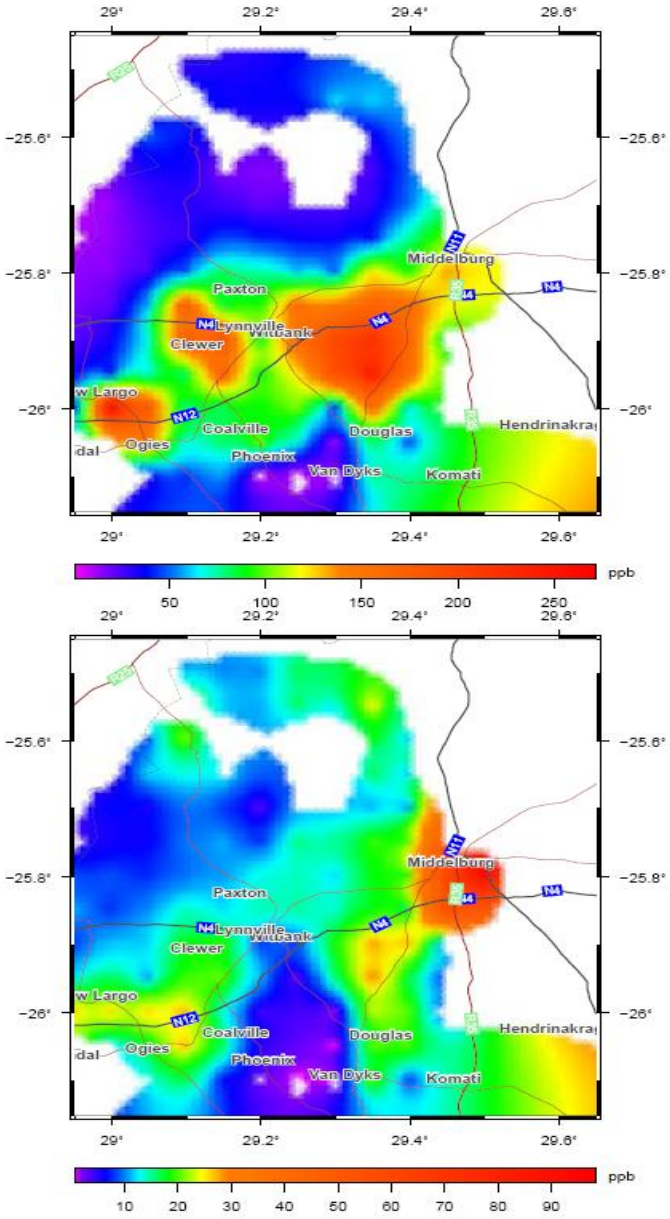


Figure 2.1: The spatial distribution of SO_2 over Witbank and surrounding towns as measured by the aircraft. The top figure shows the maximum values and the bottom figure the median values gridded on a 0.05 by 0.05 degree resolution (Piketh *et al*., 2006).

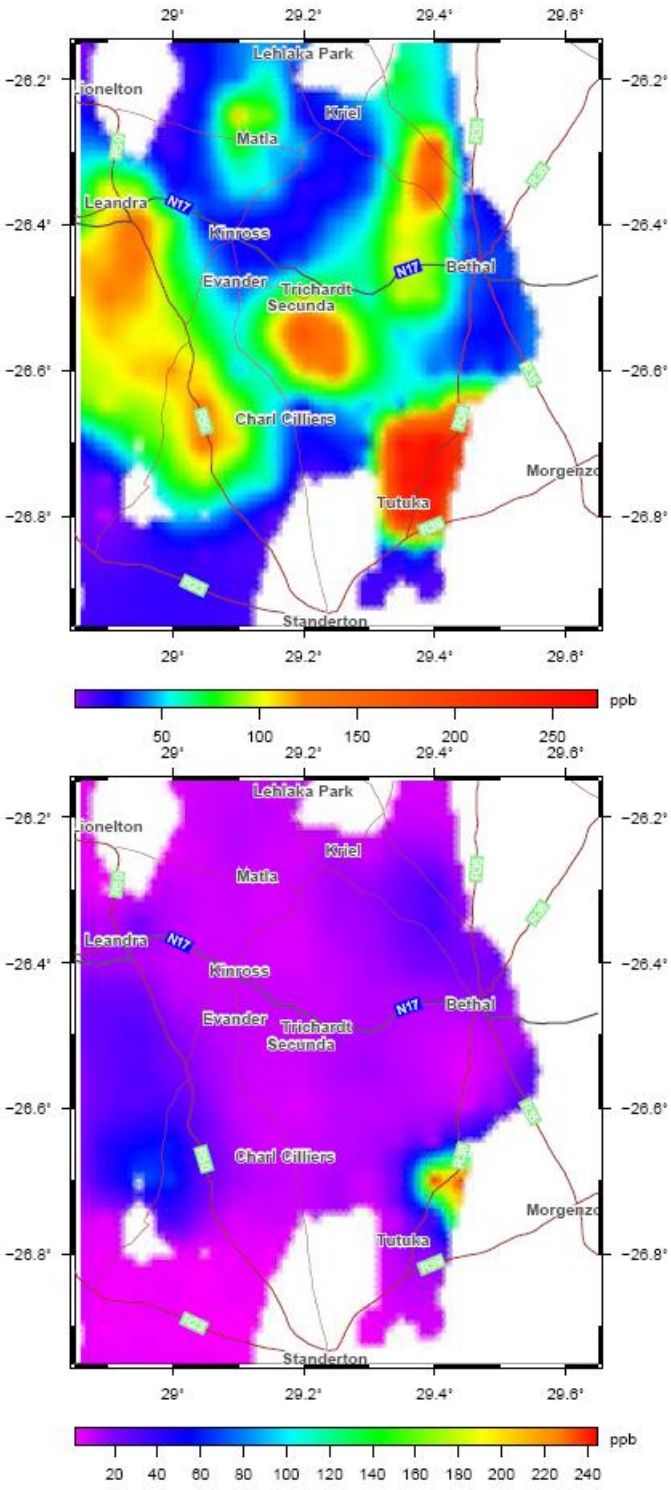


Figure 2.2: The spatial distribution of SO_2 over Secunda and surrounding towns as measured by the aircraft. The top figure shows the maximum values and the bottom figure the median values gridded on a 0.05 by 0.05 degree resolution (Piketh *et al*., 2006).

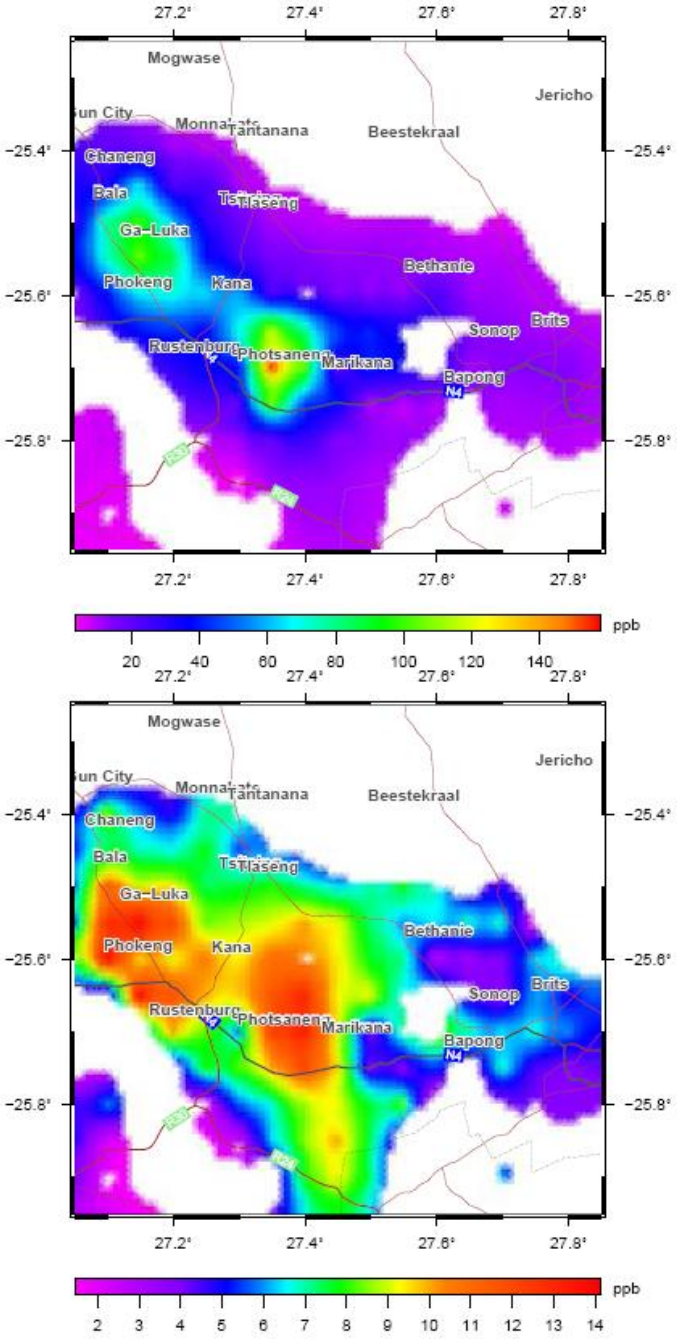


Figure 2.3: The spatial distribution of SO_2 over Rustenburg and surrounding towns as measured by the aircraft. The top figure shows the maximum values and the bottom figure the median values gridded on a 0.05 by 0.05 degree resolution (Piketh *et al*., 2006).

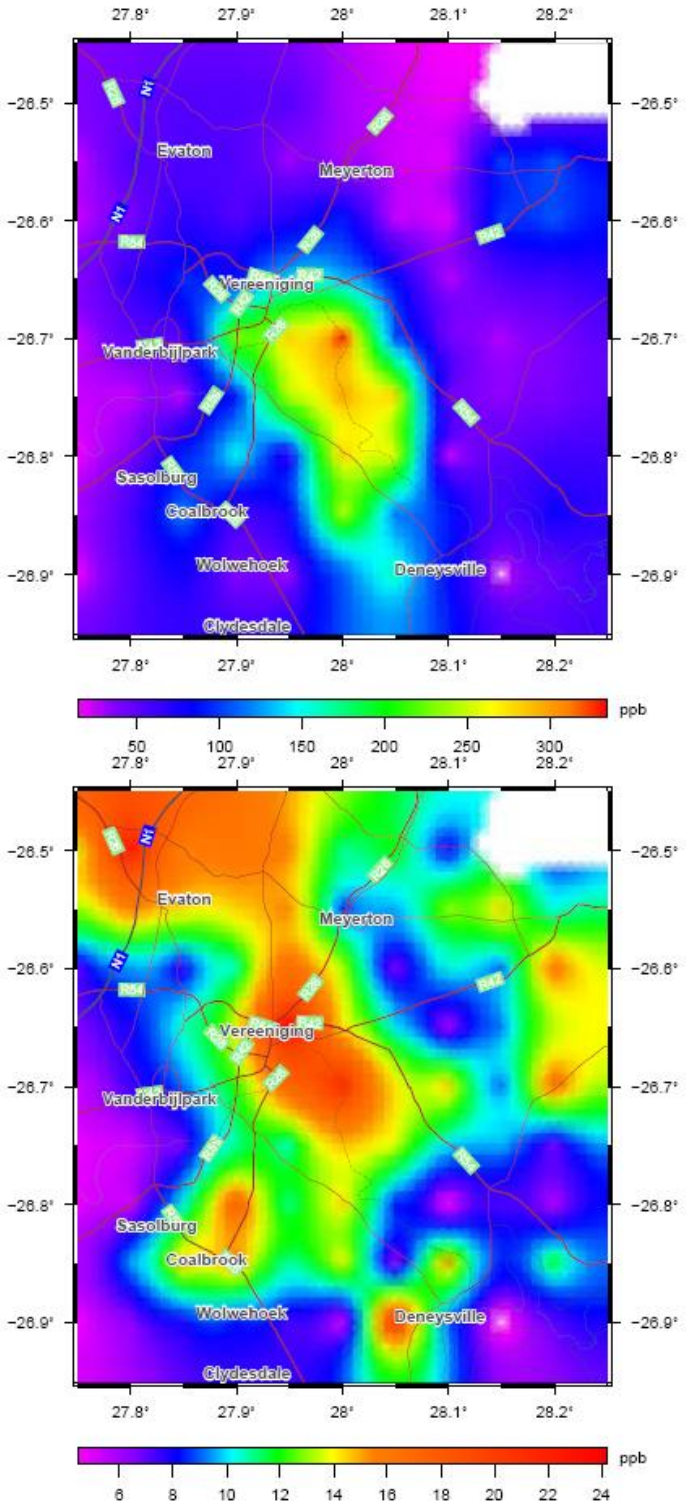


Figure 2.4: The spatial distribution of SO_2 over the Vaal Triangle area and surrounding towns as measured by the aircraft. The top figure shows the maximum values and the bottom figure the median values gridded on a 0.05 by 0.05 degree resolution (Piketh *et al*., 2006).

Research Aircraft and instruments onboard

The SAWS airocommander 690A (Figure 2.5(a)) was used as a mobile platform to monitor air pollutants over South Africa. It is capable of flying up to 30 000 ft (9.144 km) altitude and it has a flight endurance of 5.5 hours. Its weight capacity is 2500 Kg and it carried only the pilot and two operators (scientist). The Aerocommander electricity power capacity is 220V-4kW and 110V-2kW. The aircraft was equipped with the instrumentation in Figure 2.5 and Table 2.1 to measure meteorological parameters, greenhouse gases, and criteria and hazardous air pollutants.

Table 2.1: The instrumentation on board the aircraft for all the campaigns.

Parameter	Sensor
Position	Trimble TNL-200 GPS
Dynamic pressure	Rosemount
Static pressure	Rosemount
Temperature	Rosemount
Relative humidity	Vaisala Humicap
Liquid water content	Rosemount
SO_2 concentration	43C Pulsed Fluorescence SO_2 analyser
O_3 concentration	49C UV Photometric O_3 analyser
NO_X concentration	42C Chemiluminescence NO_X analyser
$PM_{2.5}$ Aerosol counter and size	PMS PCASP
Giant aerosol counter and size	PMS FSSP



Figure 2.5: SAWS research aircraft and the research equipment on onboard. Figure 2.5(a) shows the aircraft taking off from Bethlehem airfield. Figure 2.5(b) shows the aerosol probes on the nose of the aircraft, the one on the left hand side of the aircraft is for fine particles and the one on the right hand side is for coarse particles. Figure 2.5(c) shows the data acquisition system and the trace gas instrumentation onboard.

Trace gases and $PM_{2.5}$ aerosols measurement instruments

Sulphur dioxide monitor

In this study SO_2 was measured using a commercial Model 43C Trace Level fluorescence analyser. The principle of operation of the instrument is based on the fact that SO_2 molecules absorb ultraviolet (UV) light at the spectral range 190 – 230 nm and become excited at a specific wavelength, then decay to a lower energy state emitting UV light between the spectral band 240 – 420 nm (Mohn and Emmernegger, 2009; Thermo Environmental Instruments, 2009).

$$SO_2 + h\nu_1 \rightarrow SO_2^* + h\nu_2 \quad \text{..... (2.1)}$$

An air sample is drawn into the Model 43C through the sample bulkhead, as shown in Figure 2.6. The sample flows through a hydrocarbon "kicker," which filters hydrocarbons from the sample by forcing the hydrocarbon molecules to permeate through the tube wall. The SO_2 molecules pass through the hydrocarbon "kicker" unaffected. The sample flows into the fluorescence chamber, where pulsating UV light excites the SO_2 molecules. The condensing lens focuses the pulsating UV light into the mirror assembly. The mirror assembly has four selective mirrors that reflect only the wavelengths which excite SO_2 molecules. As the excited SO_2 molecules decay to lower energy states they emit UV light that is proportional to the SO_2 concentration. The band pass filter allows only the wavelengths emitted by the excited SO_2 molecules to reach the photomultiplier tube (PMT). The PMT detects the UV light emission from the decaying SO_2 molecules. The photodetector, placed at the back of the fluorescence chamber, continuously monitors the pulsating UV light source and is connected to a circuit that compensates for fluctuations in the UV light. The sample then flows through a flow sensor, a capillary, and the shell side of the hydrocarbon "kicker." The Model 43C outputs the SO_2 concentration to the front panel display as analog outputs. (Thermo electron corporation environmental instruments, 2004; Thermo Environmental Instruments, 2009).

The SO_2 monitor will measure SO_2 and any species which absorbs at about 190 – 230 nm and fluoresce at the spectral range 240 – 420nm. Several air pollutants in the atmosphere absorb UV radiation between 190 – 230 nm and fluoresce between 240 – 420 nm, for an example NO and polynuclear aromatic hydrocaborns (PAH) (Luke, 1997; Mohn and Emmernegger, 2009). The interference due to the overlapping UV light absorption bands and the fluorescence bands, may result to higher than actual SO_2 concentrations readings. The Model 43C SO_2 fluorescence analysers have hydrocarbon kicker to remove hydrocarbons from the sample air. NO fluoresces in a spectral range that is close to the SO_2 fluorescence range. Interference from NO is resolved by the presence of the band pass filter, which allows only the wavelength emitted by the excited SO_2 molecules to reach the photomultiplier tube (PMT) (Thermo Environmental Instruments, 2009). The response time of the SO_2 pulsed fluorescence sensor is low, however the instrument's effortless calibration, dependability, sensitivity, accuracy and SO_2 specifity make it preferable (WMO, 2001).

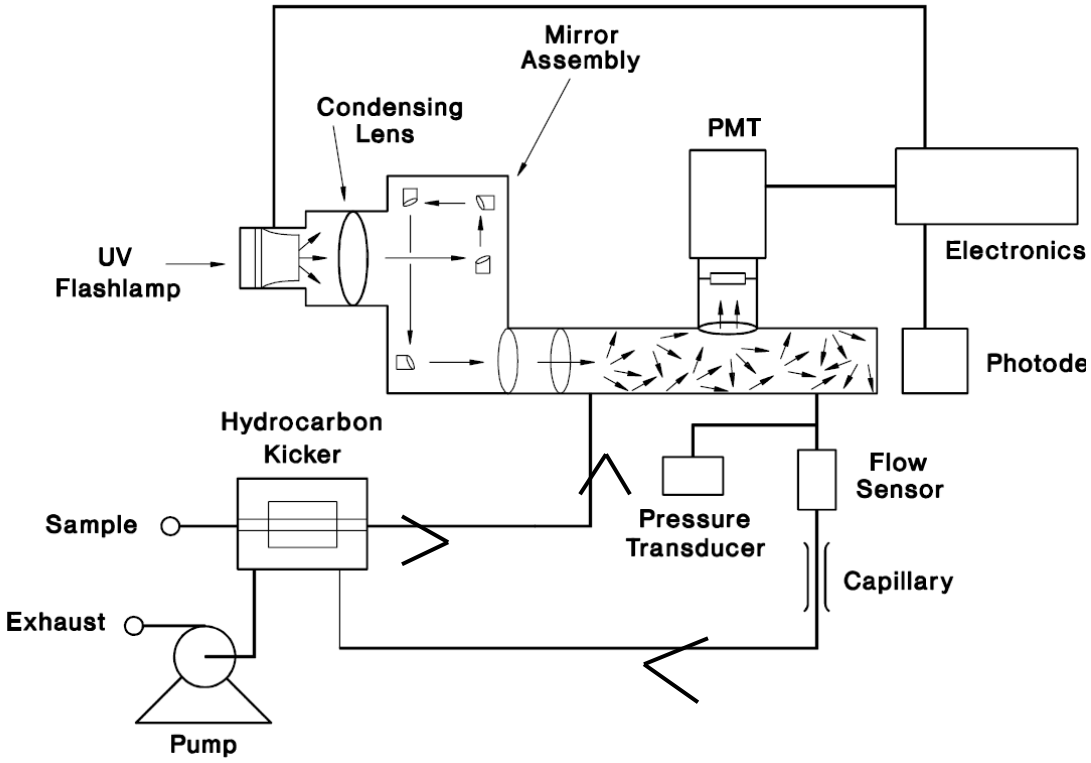


Figure 2.6: Model 43C flow diagram, Sulphur dioxide monitor (Thermo electron corporation environmental instruments, 2004).

Nitrogen oxides monitor

The NO_X were measured using Model 42C Chemiluminescence NO-NO_2-NO_x analyser. The principle of operation of the instrument is based on that NO and O_3 react to produce electronically excited NO_2^* molecule which in turn produces a characteristic luminescence with an intensity linearly proportional to the NO concentration. In this case of NO_x monitoring by chemiluminescence reaction, O_3 is the reagent added in excess to the flow of ambient air containing NO_x to be measured. The infrared light emission results when electronically excited NO_2^* molecules decay to lower energy states. (Ridley and Grahek, 1990; Thermo electron corporation environmental instruments, 2004).

NO_2 must first be transformed into NO before it can be measured using the chemiluminescent reaction. NO_2 is converted to NO by a molybdenum NO_2-to-NO converter heated to about 325 ^{0}C. The ambient air sample is drawn into the Model 42C through the sample bulkhead, as shown in Figure 2.7. The sample flows through a particulate filter, a capillary, and then to the mode solenoid valve. The solenoid valve directs the sample either straight to the reaction chamber (NO mode) or through the NO_2-to-NO converter and then to the reaction chamber (NO_x mode). A flow sensor prior to the reaction chamber measures the sample flow. Dry air enters the Model 42C through the dry air bulkhead, through a flow sensor, and then through a silent discharge ozonator. The ozonator generates the necessary ozone concentration needed for the chemiluminescent reaction. The ozone reacts with the NO in the ambient air sample to produce electronically excited NO_2^* molecules. A photomultiplier tube (PMT) housed in a thermoelectric cooler detects the NO_2^* luminescence. Chemiluminescence NO_x analysers measure NO concentration by using a band pass filter to select light in the region from about 600 to 900 nm. The NO and NO_x concentrations calculated in the NO and NO_x modes are stored in memory. The difference between the concentrations is used to calculate the NO_2 concentration. The Model 42C outputs NO, NO_2, and NO_x concentrations to both the front panel display as analog outputs (Thermo electron corporation environmental instruments, 2004; Jernigan and Dee, 2009).

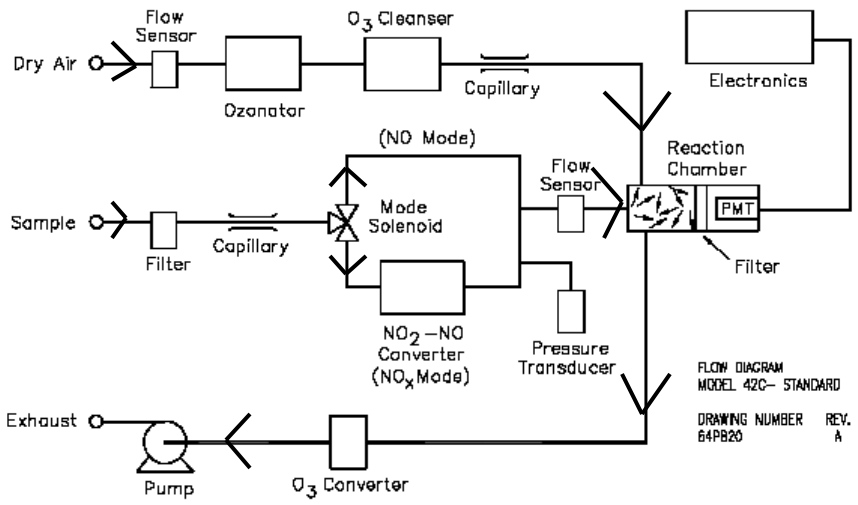


Figure 2.7: Model 42C flow diagram, Nitrogen oxides monitor (Thermo electron corporation environmental instruments, 2004).

The NO and O_3 chemiluminescence reaction mechanism is defined by the following reactions (Ridley and Grahek, 1990):

$$NO + O_3 \rightarrow NO_2^* + O_2 \quad \text{..... (2.2)}$$

$$\rightarrow NO_2 + O_2 \quad \text{..... (2.3)}$$

$$NO_2^* \rightarrow NO_2 + h\nu \ (600 \text{ nm} < \lambda < 2800 \text{ nm}) \quad \text{..... (2.4)}$$

$$NO_2^* + M \rightarrow NO_2 + M \quad \text{..... (2.5)}$$

The equations 2.2 and 2.4 describe the technique employed in commercial instrumentation to measure NO_x. Equation 2.2 describe the reaction of NO and O_3 to produce the electronically excited NO_2^* molecules. Then NO_2^* deactivates by emitting light with intensity linearly proportional to NO concentration (equation 2.4). The light emission occurs between 600 and 2800 nm, with a peak at about 1200 nm. The reactions described by equations 2.3 and 2.5, describe a potential limitation to the chemiluminescence measurement technique. Only a fraction of NO reacts to form NO_2^* and emits light. However the percentage of NO in the reactor that follows the pathway described by equation 2.2 and 2.4 is sufficient to ensure a proportionally linear response in a properly designed instrument (Jernigan and Dee, 2009).

During the process of converting NO_2 to NO by reacting NO_2 with the molybdenum (Mo) metal, Mo gets consumed in the process as follows:

$$3\,NO_2 + Mo \rightarrow MoO_3 + 3NO \quad \text{..... (2.6)}$$

The efficiency of the Mo converter degrades gradually over time. The rate of degradation is faster in polluted environment. Inefficient Mo converter results lower NO_x concentration measurements than actual NO_x levels in ambient air. Periodical service and maintenance is required for accurate NO_x concentration measurements (Doddridge *et al*., 1992; Jernigan and Dee, 2009). The advantage of Mo converter is that it can be operated at lower temperatures (325 $^{\circ}$C), hence reducing the possibility of interference by conversion of other nitrogen containing compounds to NO. Interference by conversion of other nitrogen containing compounds result high erroneous NO_x concentration measurements (Jernigan and Dee, 2009).

NO_x measurements by NO – O_3 chemiluminescence is subject to interference from large changes in absolute humidity. Water vapor decreases the instrument sensitivity by about 15%, due to more efficient quenching of the excited NO_2^* by water compared to dry air (equation 2.5) (Ridley and Grahek, 1990; Williams *et al*., 2006). The error in the NO_x measurements can be corrected to account for variations due to quenching at different levels of ambient absolute humidity by equation 2.7:

$$O_{3corr} = O_{3meas} \times (1 + 0.0043 \times WV) \quad \text{..... (2.7)}$$

Where O_{3corr} and O_{3meas} are corrected and measured O_3 concentration respectively, WV is water vapor mixing ratio in parts per thousands and the factor 0.0043 is derived from laboratory studies. The maximum correction is 15% compared to dry air (Williams *et al*., 2006).

The advantages of Chemiluminescence NO-NO_2-NO_x analyser over other measurement methods are that; it has field programmable ranges, fast response time and it is highly sensitive. It has a lower detectable limit of 0.40 ppb. The instrument is not subjected to interference by UV absorbing molecules such as aromatics. Chemiluminescence NO-NO_2-NO_x analyser offers linearity over wide dynamic range (Ridley *et al*., 1992;

Thermo electron corporation environmental instruments, 2004; Williams *et al*., 2006; Jernigan and Dee, 2009).

Tropospheric ozone monitor

O_3 was measured using Model 49C UV photometric ozone analyser. The principle of operation of the instrument is based on that ozone (O_3) molecules absorb UV light at a wavelength of 254 nm. The degree to which the UV light is absorbed is directly related to the ozone concentration as described by the Beer-Lambert Law:

$$\frac{I}{I_0} = e^{-KLC} \quad \text{..... (2.8)}$$

where:

K = molecular absorption coefficient, 308 cm^{-1} (at 0 ^{0}C and 1 atmosphere)

L = length of cell, 38 cm

C = ozone concentration in parts per million (ppm)

I = UV light intensity of sample with ozone (sample gas)

I_o = UV light intensity of sample without ozone (reference gas)

The sample is drawn into the Model 49C through the sample bulkhead and is split into two gas streams, as shown in Figure 2.8. One gas stream flows through an ozone scrubber to become the reference gas (I_o). The reference gas then flows to the reference solenoid valve. The sample gas (I) flows directly to the sample solenoid valve. The solenoid valves alternate the reference and sample gas streams between cells A and B every 10 seconds. When cell A contains reference gas, cell B contains sample gas and vice versa. The UV light intensities of each cell are measured by detectors A and B. When the solenoid valves switch the reference and sample gas streams to opposite cells, the light intensities are ignored for several seconds to allow the cells to be flushed. The Model 49C calculates the ozone concentration for each cell and outputs the average concentration to both the front panel display as analog outputs (Thermo electron corporation environmental instruments, 2004).

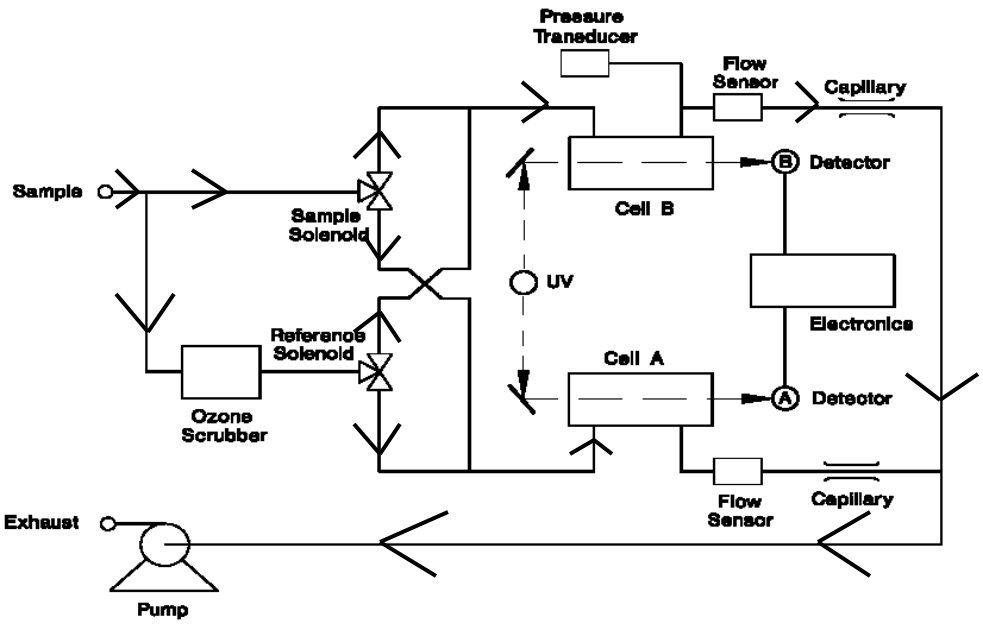


Figure 2.8: Model 49C Flow diagram, Tropospheric ozone monitor (Thermo electron corporation environmental instruments, 2004).

Since the principle of operation of O_3 UV absorbance monitor is based on absorption at 254 nm wavelength by O_3 molecules. If other species that absorb or scatter light at the same wavelength are present in the air sample and not removed by the scrubber, then the ratio $\frac{I}{I_0}$ will not reflect only the O_3 concentration, and the O_3 measurement will be in error. Aromatic volatile organic compounds and elemental mercury are known to cause interference in the UV absorption based O_3 measurement, by absorbing UV light at 254 nm cross section (Williams *et al*., 2006). The error in O_3 measurements by UV absorption instruments due to interference is considerable in highly polluted environments (Ridley *et al*., 1992; Williams *et al*., 2006).

Although the water vapor does not absorb light at 254 nm, it interferes with light transmission in optical cells with damaged dirty windows. Increased scattered light from aerosols present in the air sample but not in the scrubber air, can generate false readings. Damaged optical components and or damaged or poorly performing O_3 scrubbers have been reported to cause oscillating output. Other factors that commonly induce erroneous O_3 data include leaks and dirty or contaminated tubing, valves or optical components (Williams *et al.,* 2006).

The Model 49C UV photometric ozone analyser has field programmable ranges, fast response time and it is highly sensitive. It has a lower detectable limit of 1.0 ppb. UV absorbance O_3 monitors are preferred, especially in air quality monitoring networks, due to ease of operation, low maintenance, and because they don't need reagent gases solutions. If the UV instruments are well maintained and properly operated, they provide accurate O_3 concentration data under wide variety conditions (Thermo electron corporation environmental instruments, 2004; Williams *et al*., 2006).

$PM_{2.5}$ Aerosols monitor

This study focuses on aerosols with a diameter less than 2.5 μm. The Passive Cavity Aerosol Spectrometer Probe (PCASP) Model 100 was used to measure $PM_{2.5}$ aerosols total concentration and their particle size distributions. The instrument measures aerosols from 0.1 to 3.0 μm size range, with a concentration accuracy of $\pm$ 16% and a diameter accuracy of $\pm$ 20%. The PCASP used in this study was equipped with deicing heaters, which are intended to keep the sampling inlet ice free when super cooled clouds are encountered. The principle of operation of the instrument is based on the interaction of particles with a light beam that they pass through it. The PCASP is of that general class of instruments called optical particle counters (OPCs) that detect single particles and size them by measuring the intensity of light that the particle scatters when passing through a light beam. Figure 2.9 illustrates the optical path of this instrument. A Helium Neon laser beam is focused to a small diameter at the centre of an aerodynamically focused particle laden air stream. Particles that encounter this beam scatter light in all directions, the amount of light scattered by the sampled particle is dependent on the particle size, shape and refractive index. Some of this scattered light is collected by a mangin mirror over angles from about 35^o - 135^o. The collected light is focussed onto a photodetector and then amplified, conditioned, digitized and classified into one of fifteen size channels. The particle size is determined by measuring the light scattering intensity, and using Mie scattering theory to relate this intensity to the particle size. The size information is sent to the data system where the number of particles in each channel is accumulated over a pre-selected time period (Particle Measuring Systems (PMS), 1989; Liu *et al*., 1992; Strapp *et al*., 1992).

There are several potential sources of errors in determining sizes of particles using PCASP. Small particles are lost due to detection sensitivity and larger particles are lost in the instrument inlet walls (Garrette *et al*, 2002; Gwaze, 2006). Performance tests on PCASP – 100 found the probe to be less sensitive than what is reported by the manufacture. Liu *et al*. (1992) have found the lower detection limit of PCASP – 100 to be higher (0.125 µm) than the one reported by the manufacture (0.1 µm). The instrument determine particle sizes based on polystyrene latex (PSL) spheres with complex refractive index of $m = 1.585 - 0.0i$. Corrections need to be made for particles with different refractive indices (Garrette *et al*, 2002; Gwaze, 2006). The PCASP technique is sensitive to particle shape. The intensity of scattered light by a particle is dependent on particle shape (Lui *et al*., 1992). Deiced PCASP – 100 measure dry aerosols, the heaters of the probe burn the hydrated aerosol's moisture. Hence for deiced PCASP – 100, calibrations for refractive index changes with hydration are not applicable (Liu *et al*., 1992; Strapp *et al*., 1992). However in high relative humidity (RH) conditions where some particles might contain some water, particles might be partially evaporated, e.g, due to short residence times inside the heating column. Hence measurements might be biased, particularly for hydroscopic particles of diameters above 1 µm (Garrette *et al*, 2002; Gwaze, 2006).

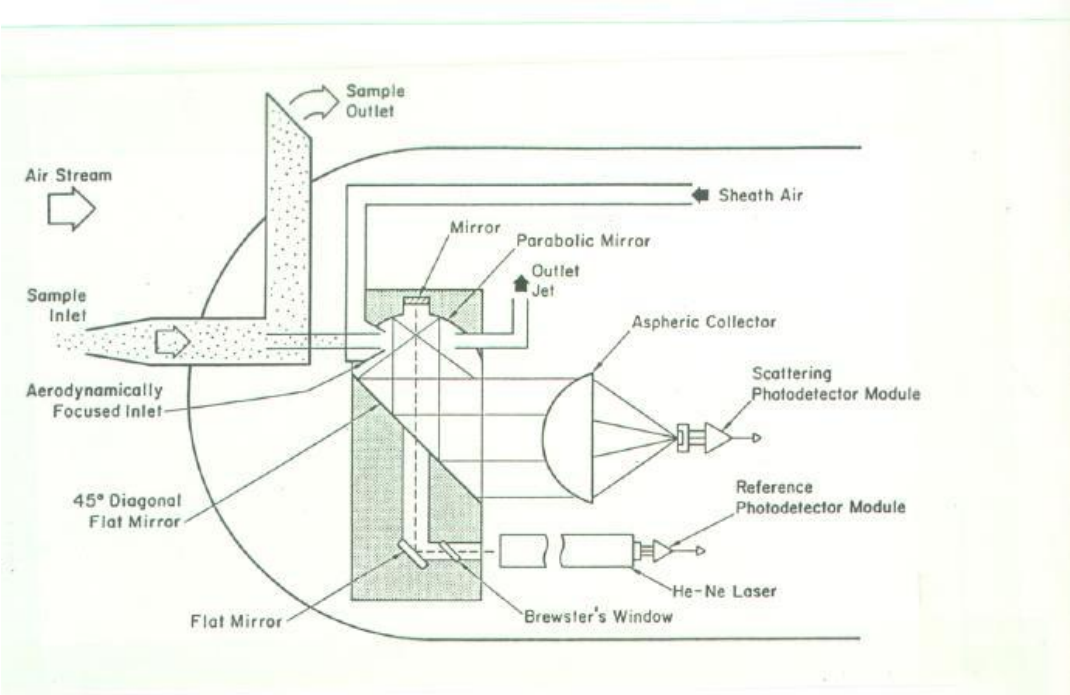


Figure 2.9: Schematic diagram of the optical path of the PCASP, $PM_{2.5}$ Aerosols instrument (PMS, 1989).

Data Collection

Airborne air pollution monitoring

Airborne air quality monitoring is a delicate operation that requires thorough cognisance of weather conditions for it to be conducted successfully. This operation requires fine weather and clear skies conditions; if clouds develop they should preferably be high lying clouds. The main reason for this is to avoid ingesting moisture from clouds into gas-phase air quality monitors. Hence for a great part of the operations, weather influenced when and where to fly. This dependence on the weather conditions affected the consistency in the time of the day at which the study sites were monitored.

For a comparison study on air pollution loading over different sites it is important that there is consistency in the time and meteorological conditions under which the sites are being monitored. Both these factors affect the levels of air pollutants in the atmosphere. This study was faced with challenges of not having all sites monitored at the same time of the day and the meteorological conditions prevailing on the days these sites were

monitored were not similar particularly for the winter campaign. For each seasonal flight campaign in this study, each site air pollution levels were directly compared to other sites provided the sites were monitored at the same time of the day. The influence of the meteorological conditions was taken into consideration when the sites were compared.

Highveld air pollution hotspots monitoring programme

The flight campaigns of this study were undertaken at different seasons of the year over the Highveld air pollution hotspots. A summary of the flight campaigns information is given in Table 2.2. Figure 2.10 shows the summary of flight patterns which were conducted over the air pollution hotspots. The flight campaigns were all based from Bethlehem airfield. Figures 2.11 to 2.14 show the mapping flight tracks that represent the areas of the Highveld air pollution hotspots.

Autumn campaign

The Highveld autumn campaign was conducted from 7 March 2005 to 18 March 2005. The campaign was based from Bethlehem airfield, and the Lanseria airfield was used as a refueling station. The Bethlehem weather office staff assisted with daily weather briefings every morning, for the purpose of deciding to fly or not to fly. In this campaign 24.3 flight hours were flown. The flight patterns were designed to do area mapping, plume or source characterization and vertical profiling. Mapping flight patterns were designed to cover these areas of interest, i.e. the Vaal Triangle area, Witbank, Secunda and Rustenburg and their close proximity surrounding sites. The area mapping flights involved 5 or more flight legs and they were conducted at approximately 167 m (500 ft) agl, 333 m (1000 ft) and 667 m (2000 ft) agl. These flights were aimed at establishing the spatial distribution of air pollutants. Figure 2.15 shows an example of an area mapping flight. Source characterisation flights were done by flying through plumes of natural and anthropogenic sources. Figure 2.16 shows an example of a source characterisation flight. Vertical profiling was done by flying an upward spiral motion to an altitude of approximately 3333 m (10000 ft) over sites of interest. These flights were intended to determine the vertical distribution of air pollutants. Figure 2.17 shows an example of vertical profiling flight.

Sampling was automatic and continuous for the aerosols and all the trace gases except for methane (CH_4) and volatile organic compounds (VOC). They were both sampled using passive sampling method. Methane was sampled into glass syringes and the VOC's into stainless steel canisters. Both were analysed at the Bethlehem base. The measurements and the data of CH_4 and the VOC's do not form part of this study.

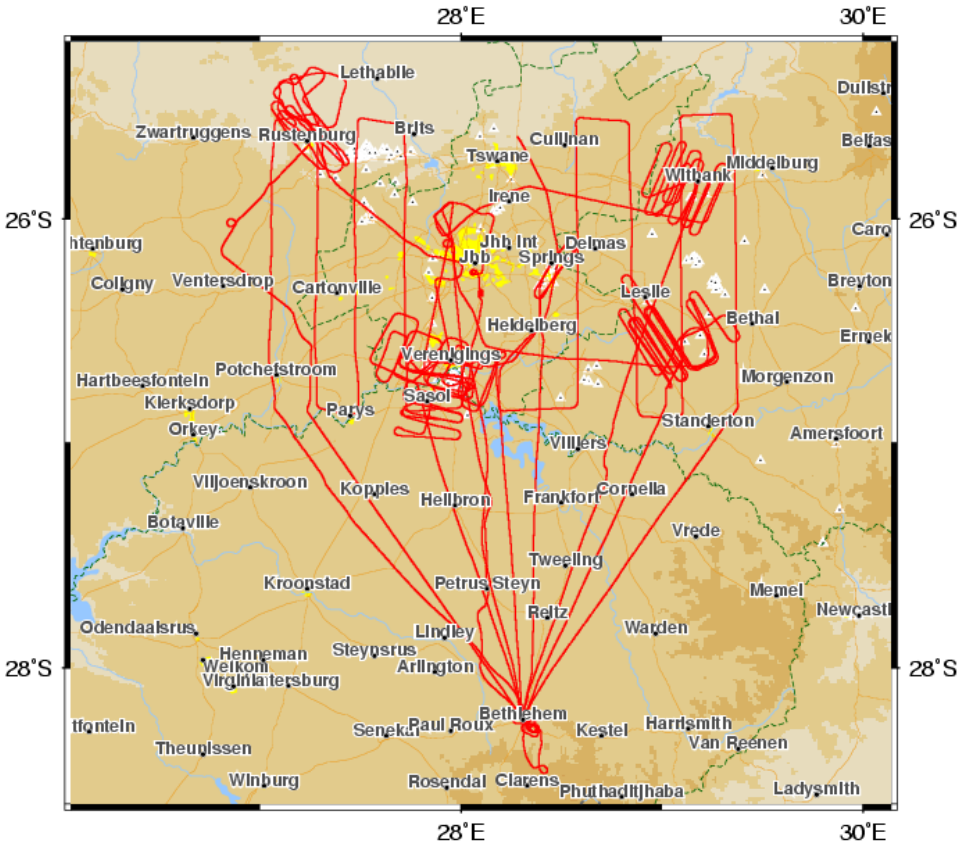


Figure 2.10: Summary of flight patterns conducted over the Highveld air pollution hotspots (Piketh *et al*., 2006).

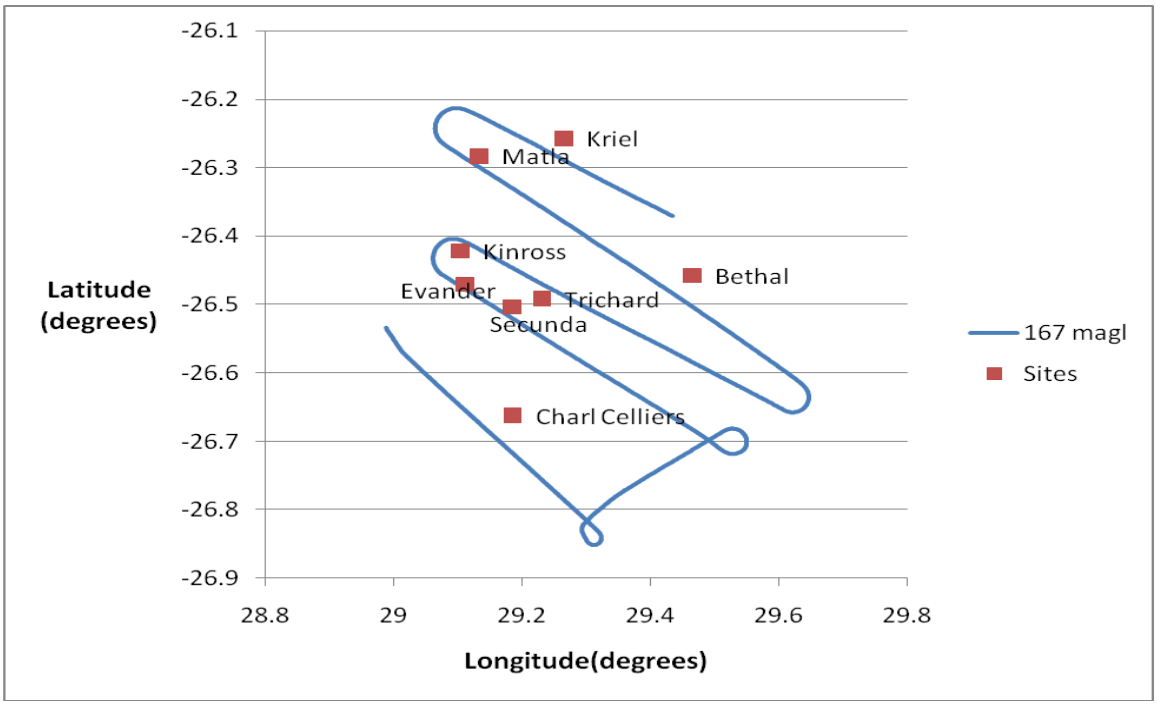


Figure 2.11: A mapping flight track representative of all the flights flown over the Secunda area at 167 magl.

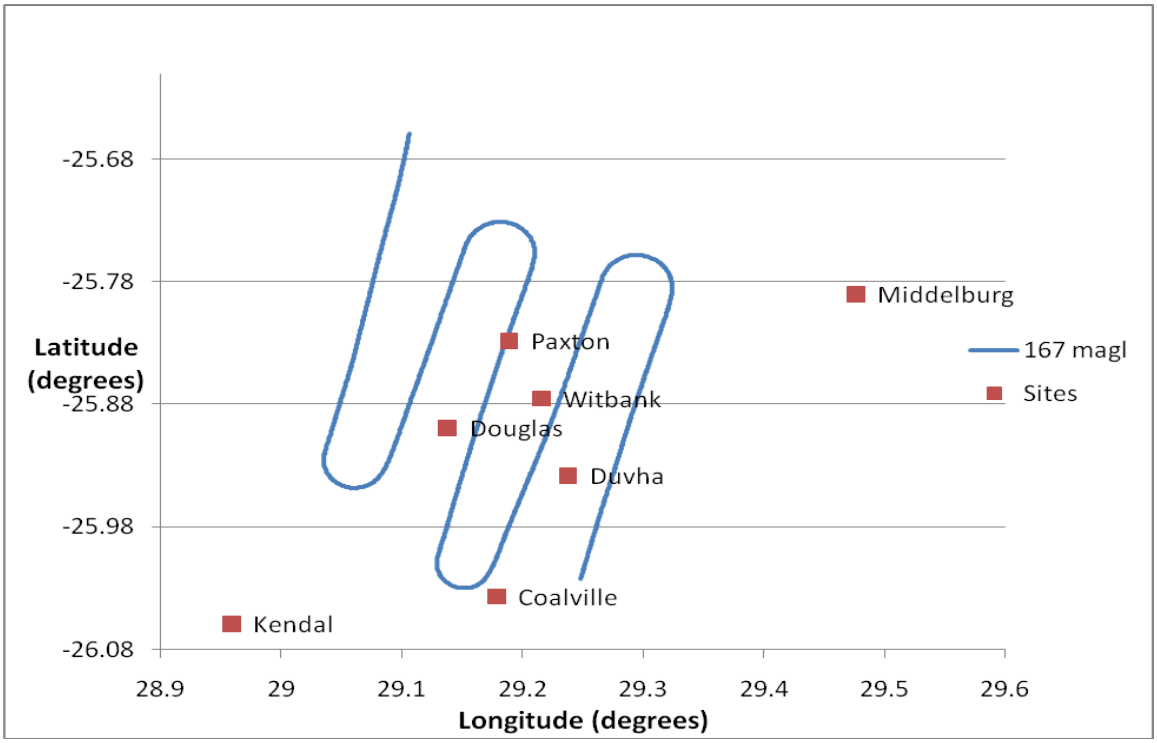


Figure 2.12: A mapping flight track representative of all the flights flown over the Witbank area at 167 magl.

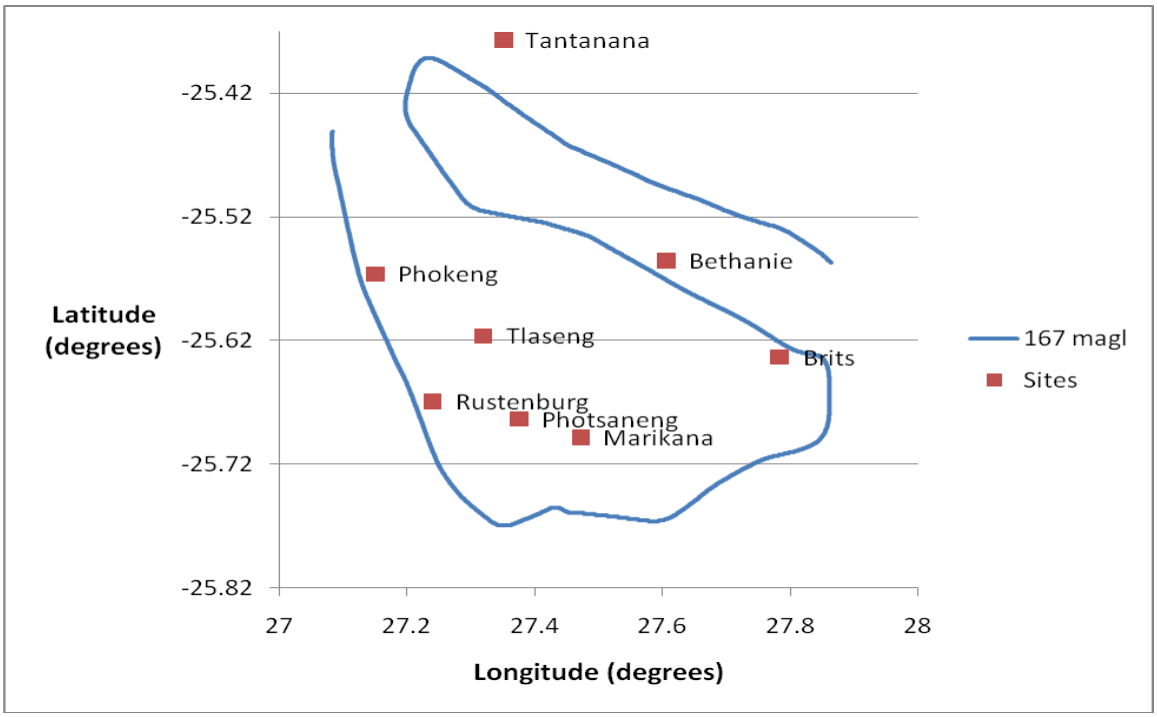


Figure 2.13: A mapping flight track representative of all the flights flown over the Rustenburg area at 167 magl.

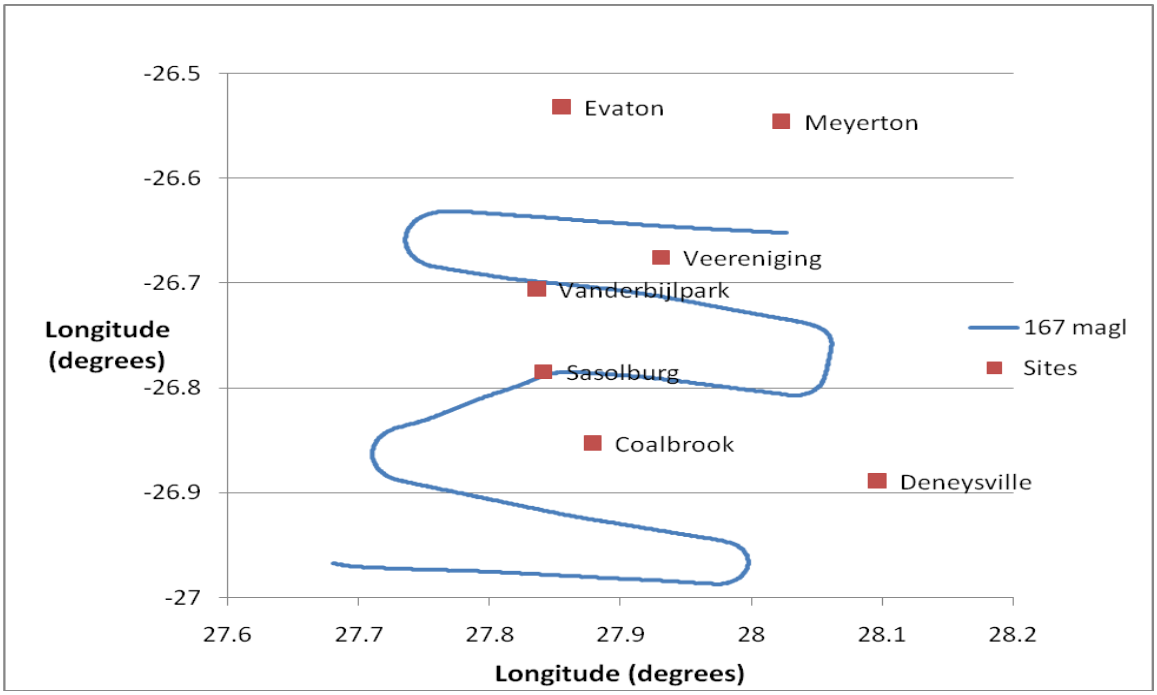


Figure 2.14: A mapping flight track representative of all the flights flown over the Vaal Triangle area at 167 magl.

Table 2.2: Highveld flight campaigns programme

Flight campaign	Date	Based from	Flight hours	Flight details
Autumn campaign	From 7 to 18 March 2005	Bethlehem	24.3	Mapping the Highveld at approximately 167 and 333 magl, plume penetration, and vertical profiles.
Winter campaign	From 19 July to 09 August 2005	Bethlehem	68.3	Mapping the Highveld at approximately 167, 333 and 667 magl, plume penetration and vertical profiling
Spring campaign	From 16 to 24 September 2005	Bethlehem	25	Mapping the Highveld at approximately 167, 333 and 667 magl, plume penetration and vertical profiling
Air pollution flux provincial cross boundary campaign	From 25 to 31 March 2006	Bethlehem	7	Vertical profile flights of up to 3 km altitude, conducted at the edges of the South African Highveld

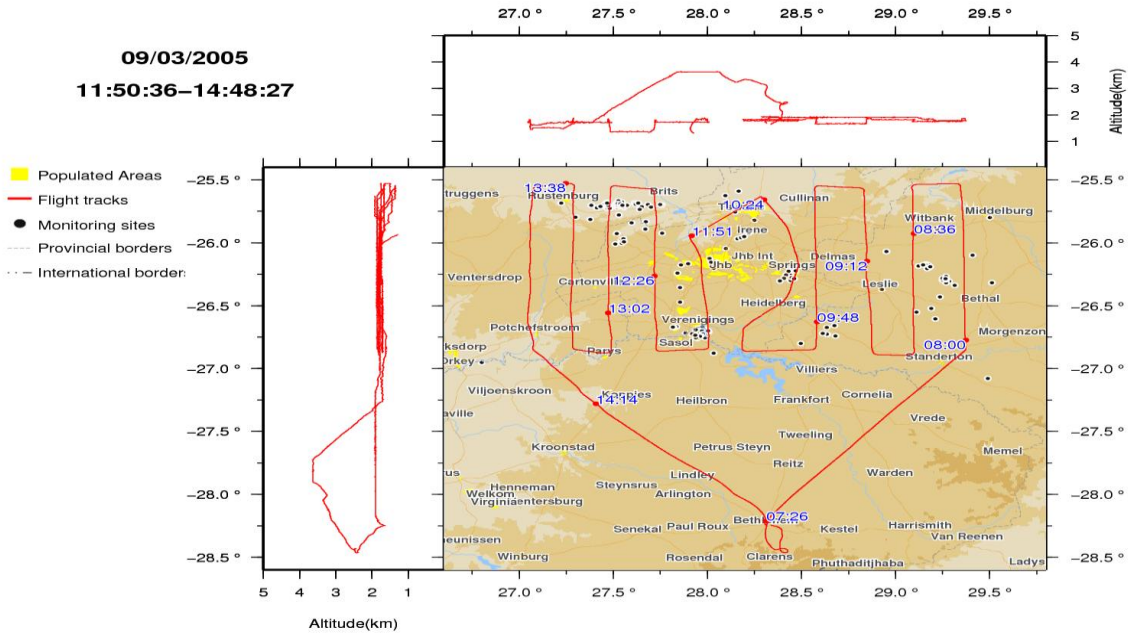


Figure 2.15: An example of a mapping flight conducted over the South African Highveld. A regular pattern with 0.5 degree longitudinal spacing was flown over the region of interest. In this example the deviation on the flight pattern was due to OR Tambo International Airport controlled airspace (Piketh *et al*., 2006).

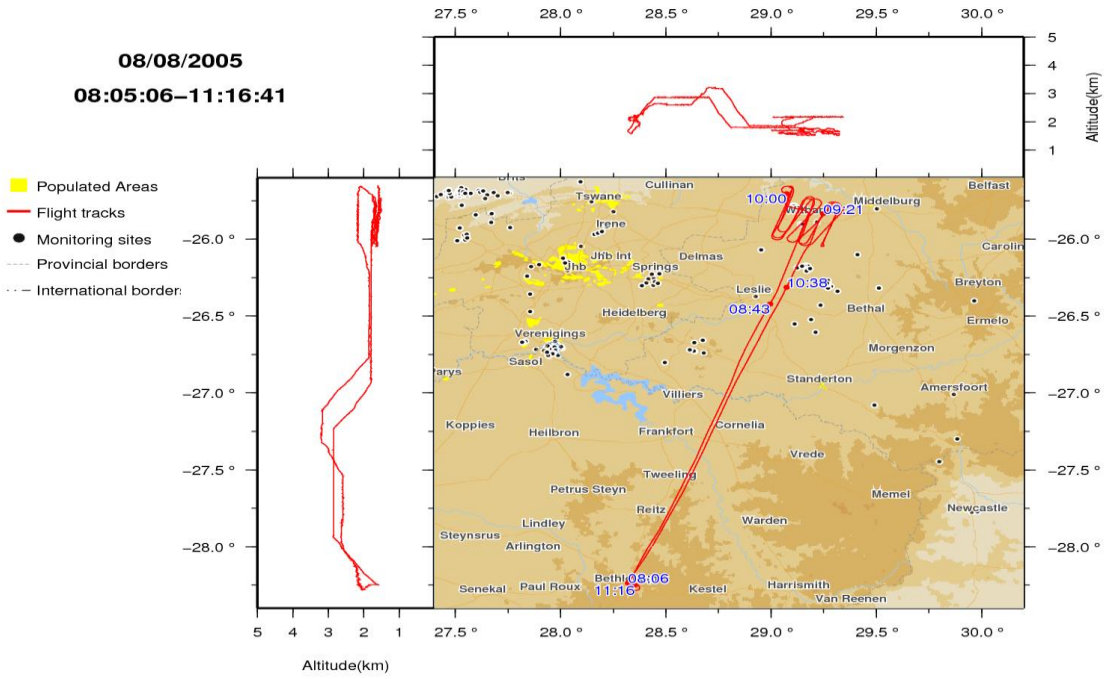


Figure 2.16: An example of a source flight conducted over the Witbank area of South Africa. The flights were conducted in the downwind direction starting and ending at the stack (Piketh *et al*., 2006).

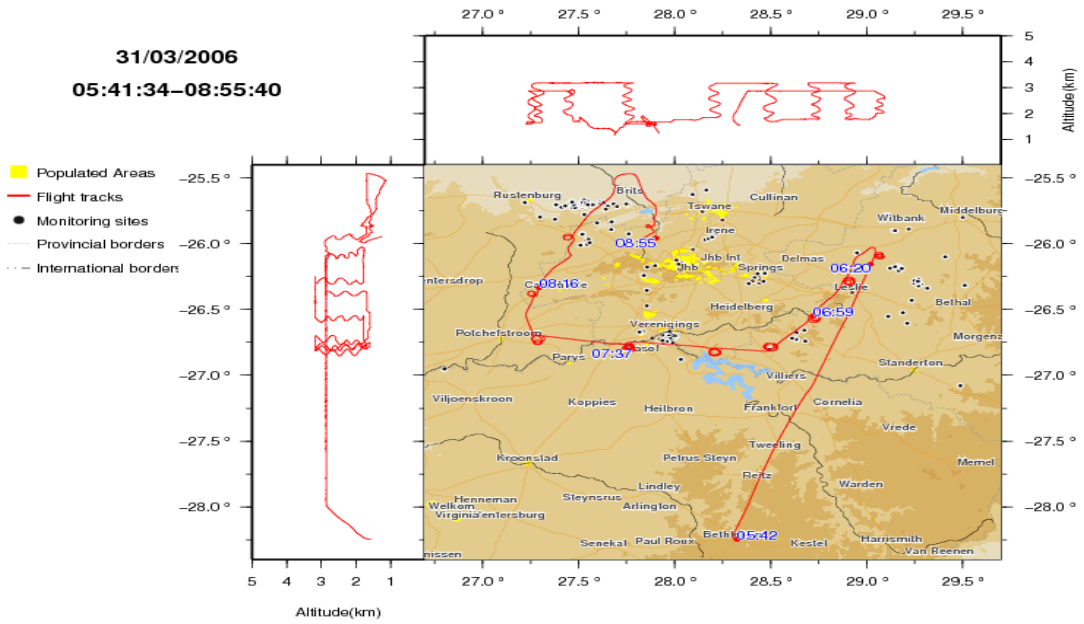


Figure 2.17: An example of profile flights conducted at the edges of the South African Highveld. The vertical extent of the flight is best viewed in the box on top of the map (Piketh *et al*., 2006).

Winter campaign

The Highveld winter campaign started on the 19 July 2005 and was concluded on 9 August 2005. It was conducted concurrently with the Durban/Richards Bay winter sampling campaign. The campaigns were both based from the Bethlehem airfield. The Lanseria airfield was again used as a refueling station, for the Highveld campaign. The Highveld component together with the Durban/Richards Bay component of this campaign consumed 68.3 flight hours. The flight patterns were similar to the ones conducted during the autumn campaign. Mapping flight patterns over the Highveld were designed to cover the areas of interest, i.e. the Vaal area, Sasolburg, Witbank, Secunda and Rusternburg. Sampling was automatic for the aerosols and all the trace gases except for methane and volatile organic compounds (VOC'S). The methane and the VOC'S were both sampled and analysed as described in the autumn campaign.

Spring campaign

The Highveld spring sampling campaign was conducted between 16 September 2005 and 29 September 2005. It was conducted concurrently with the Durban/Richards Bay spring sampling campaign. Both campaigns were based from the Bethlehem airfield. The Lanseria airfield was used as a refueling station, as in the other Highveld campaigns. The Bethlehem weather office staff, like in the other campaigns, assisted with daily weather briefings every morning. The Highveld campaign consumed 25 flight hours. Similar flight patterns and operation procedures were conducted over the Highveld study sites, as in the other campaigns.

Air pollution flux provincial cross boundary campaign

The air pollution flux provincial cross boundary campaign was conducted from 25 March 2006 to 31 March 2006. This campaign was also based in Bethlehem, it consumed 7 flight hours. The flight patterns involved in this campaign were vertical profiles up to 3 km altitude along the Highveld provincial boundaries. Figure 2.17 shows an example of the of the flight pattern conducted for this campaign. The data generated from this campaign were used in this study to show the vertical uneven distribution of pollutants caused by the release of fresh emissions at different heights.

Data analysis

Comparison of Highveld air pollution hotspots

For the comparison of baseline ambient levels of O_3, NO_X, SO_2 and $PM_{2.5}$ over the four Highveld air pollution hotspots, only the data collected at approximately 167 magl were used. This is the level that was consistently monitored at all the study sites in all the seasonal campaigns. The observations were made during the autumn, winter and spring campaign. Data from apparent industrial plume penetration were eliminated from the data set. This was achieved by sketching time series plots for each pollutant for all selected seasonal case studies, and then eliminating sharp spikes or peaks from the data set. Quartile analysis was then performed to determine the concentration distribution of O_3, NO, NO_2, SO_2 and $PM_{2.5}$ aerosols in ambient air, over the four Highveld air pollution

hotspots. Then spatial average concentrations were calculated to establish spatial average concentrations of the air pollutants in each seasonal case study.

Quartile analysis

Quartile analysis is a statistical methodology that divides observations into four defined intervals based upon the values of the data and how they compare to the entire set of observations. Each interval or quartile contains 25% of the total observations. Suppose observations of a variable are ordered by value, in an ascending order like below:

$n_1 > n_2 > n_3 > n_4 > n_5 > n_6 > n_7 > n_8 > n_9 > n_{10} > n_{11}$

The first quartile (Q_1) or lower quartile is the value in the observations such that 25% of the values are less than it and 75% greater than it. Its position in the arrangement is given by:

$$(n + 1)\left(\frac{1}{4}\right) \quad \text{..... (2.9)}$$

where n is the number of observations.

The second quartile (Q_2) or median is the value in the observations such that 50% of the values are less than it and 50% are greater than it. Its position in the arrangement is given by:

$$(n + 1)\left(\frac{1}{2}\right) \quad \text{..... (2.10)}$$

The third quartile (Q_3) or upper quartile is the value in the observations such that 75% of the values are less than it and 25% are greater than it. Its position in the arrangement is given by:

$$(n + 1)\left(\frac{3}{4}\right) \quad \text{..... (2.11)}$$

If the number of observations is odd, the Q_1, Q_2, and Q_3 position will be a whole number. If the number of observations is even, the Q_1, Q_2, and Q_3 position will include a decimal. This means that Q_1, Q_2, and Q_3 position lies between two observation values. In this case Q_1, Q_2, and Q_3 can be determined by averaging the two observation values that sandwich the calculated Q_1, Q_2, and Q_3 position (Statistics Canada, 2009a; Wolfram Research, 2009).

The QUARTILE function from Excel 2003 software was used to calculate the nth quartile values of O_3, NO_X, SO_2 and $PM_{2.5.}$ The syntax for the Quartile function is:

QUARTILE (array, nth_quartile) ……... (2.12)

array is a cell range, in this case a column of observations of a particular air pollutant, from which the nth quartile is returned.

The nth_quartile is the quartile value that you wish to return. It can be one of the following values:

Table 2.3: nth quartile values and their explanations

Value	Explanation
0	Smallest value in the data set (minimum)
1	First quartile
2	Second quartile
3	Third quartile
4	Largest value in the data set (maximum

Remarks

- If array is empty, Quartile returns the #NUM! error value.
- If quart is not an integer, it is truncated.
- If quart < 0 or quart > 4, QUARTILE returns the #NUM! error value.
- MIN, MEDIAN, and MAX return the same value as QUARTILE when quart is equal to 0 (zero), 2, and 4, respectively (Tech on the Net, 2008).

The quartile analyses were performed on the data collected at 167 magl over the study sites whose area sizes are represented by Figure 2.11 to Figure 2.14.

Spatial average concentration

In mathematics and statistics, the arithmetic mean (or simply the mean) of a list of numbers is the sum of the list divided by the number of items in the list. If a data set is denoted by $x = (x_1, x_2, ..., x_n)$, then the sample mean is typically denoted with a horizontal bar over the variable $\bar{x}$ and is given by the expression (Statistics Canada, 2009b):

$$\bar{x} = \frac{1}{N}\sum_{i=1}^{N} x_i \quad \text{..... (2.13)}$$

The spatial average concentrations at different flight levels were calculated for data collected over the Highveld air pollution hotspots, whose areas sizes are represented by Figure 2.11 to Figure 2.14.

Meteorological data

The SAWS 1400 SAST (1200UT) synoptic surface charts, surface and upper air data were used to assist in the interpretation of analysed air quality data and to highlight the influence of meteorological conditions during different seasons on air pollution levels. Only the Secunda site did not have a weather station which is observing 24 hours during the period of this project. For this study data from the nearest stations, Witbank and Ermelo which are about 71 km north and 78 km east of Secunda respectively (Google Earth, 2010a) were used to infer the likely atmospheric conditions at Secunda. Irene (Pretoria) weather station's upper air data were used to characterise the vertical structure of the lower column of the troposphere and to monitor the diurnal evolution of the mixing layer. Data from this station were selected because of the station being in proximity (Brooks *et al.,* 1994; Craven and Brooks, 2004; Groenemeijer and van Delden, 2007; Brooks, 2009) and centrally located in relation to the four study areas, and as the region is relatively flat (Coutsoukis, 1996; WWF, 2001). Irene is about 100 km away from the study sites, except Secunda which is about 120 km away (Google Earth, 2010b). The temperature vertical profile from this station may not be the exact match to the profiles at the study areas, but it could be considered to be representative of the region. The heights above ground level of the temperature vertical profiles were calculated by subtracting the

altitude of the surface at Irene weather station from the altitude of the sensor at each point of its ascent:

Height(magl) = Altidude(asl) – Altitude(surface)…… (2.14)

Comparison of airborne and surface air pollution data

The comparability of airborne air quality data to surface measurements is dependent on the degree of mixing of air in the troposphere. The mixing is in turn influenced by meteorological conditions, atmospheric lifetime of air pollutants, sources distribution and the height at which the pollutants are released into the troposphere (Annegarn *et al.*, 1996a; Luke *et al*., 1998). The agreement between airborne and surface air quality data is strongly influenced by the diurnal evolution of the mixing layer (Luke *et al*., 1998). In the morning the surface emissions are trapped below a shallow mixing layer caused by the nocturnal ground level inversion, and emissions from tall industrial stacks are prevented from mixing with the air below this inversion. This results in a vertical gradient in air pollutants concentration distribution. By midday the surface inversion is eroded and the mixing layer is deep enough to allow air aloft to mix with surface air. This leads to a deep mixing layer with air homogeneously mixed in vertical up to high altitudes (Annegarn *et al*., 1996a; Luke *et al*., 1998). Once mixing has taken place it is then a good time to compare the two data sets (Luke *et al*., 1998).

Stagnant conditions which are characterised by light surface winds with variable direction (Scheifinger, 1992), may also favour the comparison of airborne and ground based air quality data (Luke *et al*., 1998). Under high pressure conditions accompanied by light variable winds, air in remote or rural sites not being recently influenced by air from urban area or point sources is homogeneously mixed over a wide spatial area. This condition favours agreement between airborne and ground based air quality data within the mixing layer. Strong wind conditions can bring about the opposite condition. They channel urban or point source plumes to the direction of their flow, resulting in a horizontal spatial air pollutants concentration gradients. This spatial variation in air pollutants concentration can lead to disagreement between airborne and surface measurements, even within several km of the site (Luke *et al*., 1998).

Comparison of airborne and ground based air quality data can be a challenge in an urban population centre. Urban sites are characterised by an uneven distribution of air pollutant sources, with emissions varying temporally. This occurs even when meteorological conditions supporting a homogeneous mixing of air (high pressure and light variable winds) prevail. Fresh emissions from these sources will create horizontal and vertical gradients in concentration distribution of air pollutants (Luke *et al*., 1998). Another factor that complicates the comparison of the two data sets is the atmospheric lifetime of air pollutants. Some air pollutants like O_3 for instance have a relatively long atmospheric lifetime of 28 days, as a result it is more uniformly distributed in space as compared to short lived pollutants like NO_X and SO_2, with atmospheric residence times of a day and a week respectively (Luke *et al*., 1998; Seinfeld and Pandis, 2006).

For a direct comparison of airborne and surface air quality data, only the airborne data that was collected in the vicinity of the ground based air quality monitoring sites was used. The airborne data used for the comparison of the two monitoring platforms was only considered when the aircraft was flying within a 20 km radius from the ground based monitoring sites. Since the main objective of the project was to establish baseline ambient conditions for air pollutants over air pollution hotspots. All the flights were primarily aimed at determining spatial distribution of air pollutants. Hence opportunities of flying within 20 km radius from a ground station were few. The air pollutants compared from the two data sets are O_3, and SO_2. There were no good airborne data for NO_X for the few instances when we flew within 20 km radius from the ground station. The $PM_{2.5}$ aerosols data from the two platforms were not compared, because of different measurement units from each platform, airborne data reports $PM_{2.5}$ particles levels as number concentration ($\#/cm^3$) and ground based monitoring stations as mass concentration ($\mu g/m^3$).

The Figures 2.18 to Figure 2.20 show the spatial relationship between the aircraft flight tracks relative to the positions of the ground based air quality monitoring stations that belong to Mittal Steel and Sasol industries. Figure 2.18 represents flights over the Mittal Steel and Sasol ground based stations during the Vaal Triangle monitoring, approximately at 167 magl and 333 magl flight levels. The flights were conducted on 17/03/2005 and 03/08/2005 in the afternoon. In Figure 2.19 the aircraft was flying over Sasol ground based stations during the monitoring of Secunda and the surrounding towns. The flight was conducted during the autumn campaign on 18/03/2005 in the morning. It was conducted on three flight levels, which were approximately at 167 magl, 333 magl, and 667 magl flight levels. Figure 2.20 is derived from a Western Highveld mapping flights. The flights were conducted during the winter campaign on 21/07/2005 and 25/07/2005 approximately at 333 magl. In these flights the aircraft flew over Sasol ground based stations.

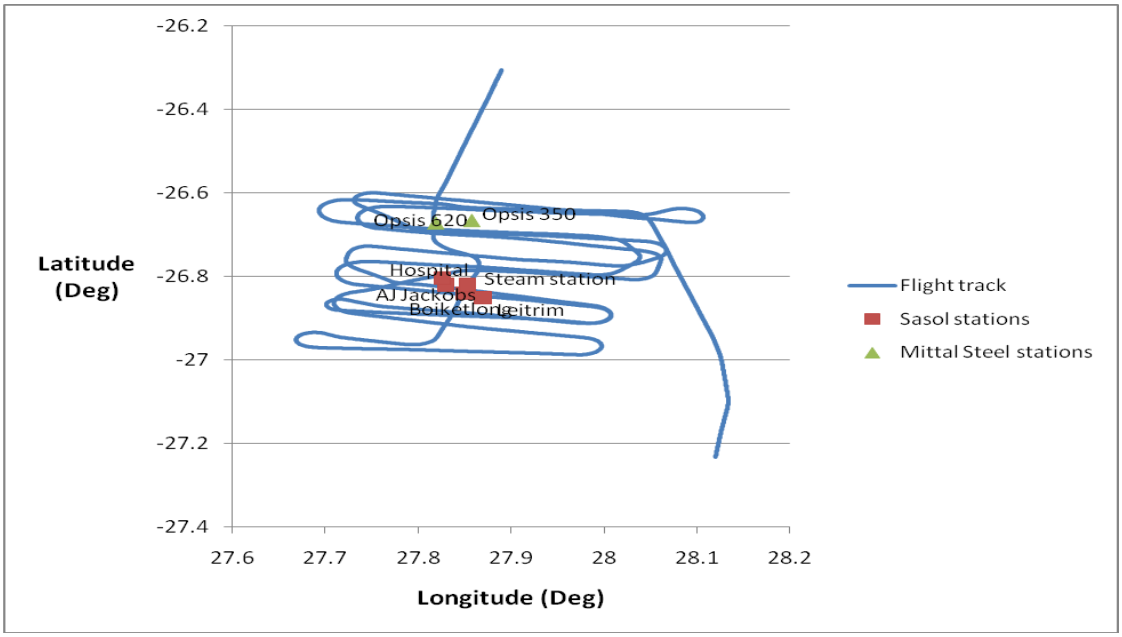


Figure 2.18: Mapping flight pattern over Sasol and Mittal Steel ground stations during the Vaal Triangle monitoring on 17/03/2005 and 03/08/2005.

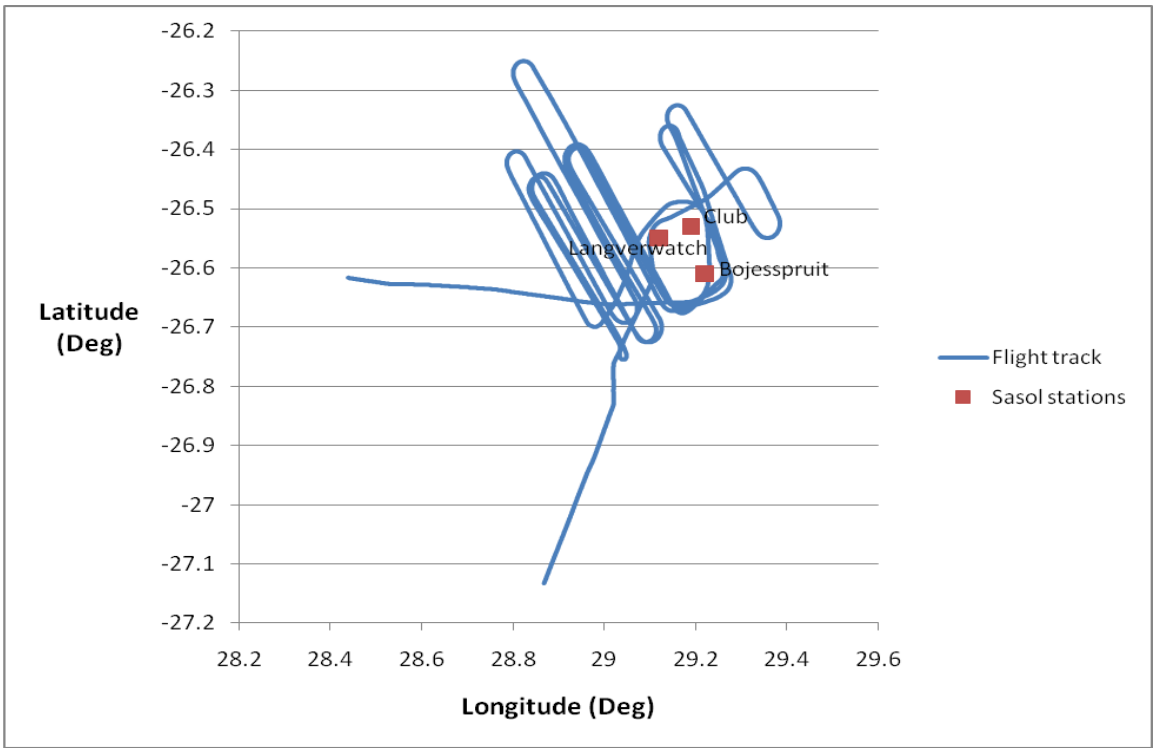


Figure 2.19: Flight over Sasol ground stations during Secunda monitoring on 18/03/2005.

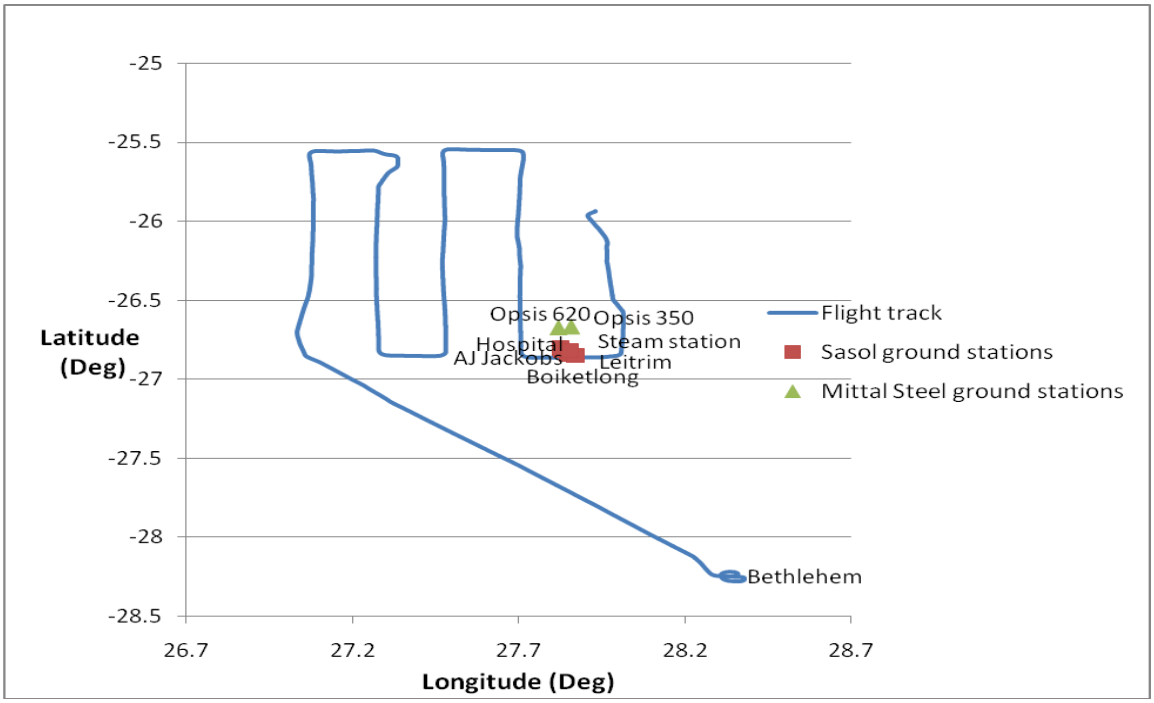


Figure 2.20: Mapping flight pattern over Sasol monitoring sites during the Western Highveld monitoring conducted on 21/07/2005 and 25/07/2005.

The ground based data is hourly averaged data from Sasol and Mittal Steel air pollution monitoring sites and the airborne data are instantaneous measurements. Because of the unavailability of high resolution temporal ground based data. Airborne data was compared with an hour average and the month average of that specific hour that correspond to a time the aircraft flew within 20 km radius from a ground station. The variability of the ground based data was determined by calculating the monthly standard deviations, using a specific hour that correspond to a time the aircraft flew within 20 km radius from a ground station. The standard deviation is given by:

$$S = \sqrt{\frac{1}{N}\sum_{i=1}^{N}(x_i - \bar{x})^2} \quad \text{..... (2.15)}$$

Where S is the standard deviation, N is the number of observations, x_i is a member of a finite data set, and $\bar{x}$ is the arithmetic average of the data set (Statistics Canada, 2009b). The observations of the airborne data used to compare the two platforms were made during the autumn and winter field campaigns.

****

Methodologies used to collect data were presented. The instrumentation and their principle of operation were described in detail. The statistical method that was used to analyse air quality data is discussed and the meteorological data that were used to assist in the interpretation of analysed air quality data were also mentioned. Challenges in comparing airborne data and ground based data are mentioned. The analysis of air quality data for comparing the air pollution hotspots and their interpretation will be discussed in the next chapter.